Journal of Applied Polymer Science

Effect of graphene oxide on the behavior of poly(amide-6-b-ethylene oxide)/graphene oxide mixed-matrix membranes in the permeation process

Dan Zhao,[1,2] Jizhong Ren,[1] Yongtao Qiu,[1,2] Hui Li,[1] Kaisheng Hua,[1] Xinxue Li,[1] Maicun Deng[1]

[1]National Laboratory for Clean Energy, Dalian Institute of Chemical Physics, Chinese Academy of Sciences, 457 Zhongshan Road, Dalian 116023, China

[2]University of Chinese Academy of Sciences, Beijing 100049, China

Correspondence to: J. Ren (E-mail: renjizhong@dicp.ac.cn)

ABSTRACT: Polyether-*block*-amide (Pebax)/graphene oxide (GO) mixed-matrix membranes (MMMs) were prepared with a solution casting method, and their gas-separation performance and mechanical properties were investigated. Compared with the pristine Pebax membrane, the crystallinity of the Pebax/GO MMMs showed a little increase. The incorporation of GO induced an increase in the elastic modulus, whereas the strain at break and tensile strength decreased. The apparent activation energies (E_p) of CO_2, N_2, H_2, and CH_4 permeation through the Pebax/GO MMMs increased because of the greater difficulty of polymer chain rotation. The E_p value of CO_2 changed from 16.5 kJ/mol of the pristine Pebax to 23.7 kJ/mol of the Pebax/GO MMMs with 3.85 vol % GO. Because of the impermeable nature of GO, the gas permeabilities of the Pebax/GO MMMs decreased remarkably with increasing GO content, in particular for the larger gases. The CO_2 permeability of the Pebax/GO MMMs with 3.85 vol % GO decreased by about 70% of that of the pristine Pebax membrane. Rather than the Maxwell model, the permeation properties of the Pebax/GO MMMs could be described successfully with the Lape model, which considered the influence of the geometrical shape and arrangement pattern of GO on the gas transport. © 2015 Wiley Periodicals, Inc. J. Appl. Polym. Sci. **2015**, *132*, 42624.

KEYWORDS: gas transport; graphene oxide; mixed matrix membranes; pebax

Received 17 March 2015; accepted 15 June 2015

DOI: 10.1002/app.42624

INTRODUCTION

Membrane-based processes have been used in various applications, such as chemical processing, energy production, and environmental protection. Membranes can be prepared with many methods. The most applied technique for the preparation of homogeneous membranes is solution casting.[1] For asymmetric membranes, it includes the dip-coating[2] and phase-inversion techniques.[3,4] For different applications, some modifications of the membrane are usually needed; these include blending, cross-linking, and grafting. Among these, mixed-matrix membranes (MMMs), a blend of organic polymers and inorganic fillers, have drawn considerable attention because they can combine the advantages of polymers and inorganic materials,[5] and they have been widely researched for the separation of O_2/N_2,[6] CO_2/CH_4,[1] and so forth.

To improve the membrane performance, some fillers, such as zeolites, carbon molecular sieves, metal organic frameworks, and carbon nanotubes, have been used to prepare MMMs.[7–10] In addition to these permeable fillers, impermeable fillers, such as SiO_2, TiO_2, and C_{60}, have also been investigated.[11–13] In recent years, nanocomposites and MMMs based on flake fillers such as graphene have attracted more attention. Compared with traditional molecular-sieving materials, flake fillers usually have a high aspect ratio (A_f), which is favorable for the preparation of thin MMMs.

Graphene is a two-dimensional carbon monolayer composed of sp^2-hybridized carbons, and graphitic materials of all other dimensionalities can be built with graphene, such as fullerene (zero dimensional), carbon nanotubes (one dimensional), and graphite (three dimensional).[14] Graphene has very strong mechanical properties[15] and is impermeable to all gases.[16]

Nanocomposites containing graphene have been used in a variety of applications, such as those in electricity,[17,18] mechanics,[19] separation,[17,20] and catalysts.[21] It has been pointed out that the mechanical enhancement of nanocomposites can be achieved when graphene is dispersed homogeneously in the polymer matrix and the interfacial interactions between the fillers and the polymer matrix is strong.[19] However, because of the

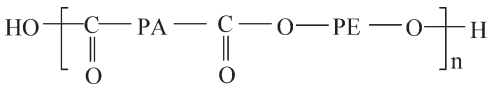

Figure 1. Schematic diagram of Pebax.

intrinsic van der Waal forces, graphene tends to agglomerate; this can usually weaken the reinforcement of the nanocomposites. The functionalization of graphene, such as oxidation, can effectively reduce its agglomeration in the polymer matrix. Graphene oxide (GO) can be synthesized from graphite by Hummer method.[18,21] GO is heavily oxygenated, and its oxygen-containing functional groups include hydroxyls, epoxides, diols, ketones, and carboxyls; these can make GO strongly hydrophilic and give it a good dispersion in water.[22] In addition, the functional groups are also beneficial for the improvement of the interfacial interaction between the fillers and the polymer matrix.[23] Some studies have shown a reinforcement effect of graphene.[19,24,25] Liang *et al.*[19] achieved a 76% increase in the tensile strength and a 62% improvement in Young's modulus for poly(vinyl alcohol)/GO MMMs with 0.7 wt % GO. Steurer *et al.*[25] found that the Young's modulus of polyamide 6/thermally reduced graphite oxides nanocomposites increased by 32%, whereas the strain at break decreased by 94% with 5 wt % thermally reduced graphite oxide.

The permeation properties are very important for MMMs and can be affected by the physical and chemical properties of the fillers. For graphene, because of its impermeability to all gases and its high surface area, its incorporation into polymers creates a large barrier effect for gas diffusion.[17,26,27] Kim *et al.*[17] modified polyurethane with thermally reduced graphite oxide via melting compounding and solvent blending and found that the N_2 permeability decreased by about 50 and 80%, respectively, at 1.6 vol % thermally reduced graphite oxide; this indicated that solvent blending was more effective. Kim and Macosko[27] observed a 47% decrease in the H_2 permeability when 6.1 vol % graphite was added to poly(ethylene-2,6-naphthalate).

Polyether-*block*-amide (Pebax) is a commercial thermoplastic elastomer, and it is known for its prior penetration of CO_2 over other light gases, such as H_2, N_2, and CH_4. The general chemical structure of Pebax is shown in Figure 1, where PA is the polyamide block [e.g., as nylon 6 (polyamide 6) and nylon 12 (polyamide 12)] and PE is the polyether block [e.g., poly(tetramethylene oxide) and poly(ethylene oxide)].[28] The gas-permeation properties of Pebax have been studied,[28,29] and some modifications aimed at improving its permeabilities and selectivities, have also been made.[30–33] The modifiers are mainly organic materials, such as poly(ethylene glycol) (PEG) and poly(dimethyl siloxane) (PDMS). Car *et al.*[31,32] modified Pebax with PEG and found that the CO_2 permeability and permeation flux of the Pebax/PEG membrane (50 wt % PEG) increased by two to three times compared to those of pristine Pebax. Reijerkerk *et al.*[30] prepared Pebax/PDMS–PEG blend membranes and found that the CO_2 permeability increased by five times at a 50 wt % PDMS–PEG loading. Recently, the modification of Pebax with inorganic materials has attracted some attention, but the research on this area is still limited, and more investigations are needed.

As mentioned previously, different kinds of fillers, including permeable/impermeable fillers and organic/inorganic fillers, have been used for preparing MMMs. So, it is necessary to describe and explain the influence of different fillers on the MMMs permeation properties; these can guide and optimize the separation performance of the MMMs.

In this study, GO was incorporated into the Pebax matrix to prepare the Pebax/GO MMMs with a solution casting method. The Pebax/GO MMMs were characterized by X-ray diffraction (XRD), Fourier transform infrared (FTIR) spectroscopy, scanning electron microscopy, and stress–strain tests. Moreover, the influence of the GO content on the gas-permeation performance of the Pebax/GO MMMs was investigated. We determined the transport properties of the Pebax/GO MMMs by considering the geometrical shape and arrangement pattern of GO.

THEORY

The widely accepted theory for gas transport in dense membranes is that it is done through a solution–diffusion mechanism.[34] Some theoretical models have been developed to predict the gas permeabilities of MMMs. The steady-state permeabilities of MMMs can generally be estimated by the Maxwell model,[35] shown in eq. (1), which is suitable for the prediction of MMMs filled with molecular sieves and other polymers, in particular for those filled with low contents of spherical fillers:

$$\frac{P_{MMMs}}{P_0}=\frac{P_f+2P_0-2\phi(P_0-P_f)}{P_f+2P_0+\phi(P_0-P_f)} \quad (1)$$

$$\frac{P_{MMMs}}{P_0}=\frac{2-2\phi}{2+\phi} \quad (2)$$

$$\frac{P_{MMMs}}{P_0}=\frac{1+2\phi}{1-\phi} \quad (3)$$

where P_0 is the permeability of the pristine polymer membrane (Barrer), P_{MMMs} is the permeability of the MMMs (Barrer), P_f is the permeability of the fillers (Barrer), and ϕ is the volume fraction of the fillers. P_{MMMs}/P_0 is called the normalized permeability. When the fillers, such as C_{60}, SiO_2, are impermeable (i.e., $P_f=0$), the Maxwell model can be rewritten as eq. (2). If the fillers are highly permeable, $P_f=\infty$ can be assumed, and the result is shown in eq. (3).

For fillers with special geometries that are significantly different from a spherical one, the gas permeabilities may deviate from the predication of eq. (1). For MMMs composed of impermeable flakes, the impermeable flakes have a much larger effect on the gas permeabilities when they are parallel to the membrane surface. When ϕ of the flakes is small ($\phi << 1$) and $A_f\phi > 1$, P_{MMMs}/P_0 can be described by the Lape model[36] shown in eq. (4):

$$\frac{P_{MMMs}}{P_0}=\left(1+\frac{1}{4}\frac{A_f^2\phi^2}{1-\phi}\right)^{-1} \quad (4)$$

where A_f is used to characterize the geometrical shape of the filler and is defined as the flake length (d) divided by the thickness (h). This model assumes that the flakes are placed in a regular array, as shown schematically in Figure 2.

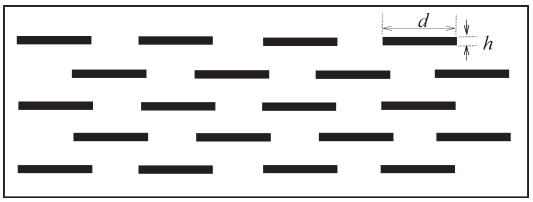

Figure 2. Schematic diagram of the Lape model.

The models mentioned previously do not consider the structural changes of the membrane induced by the fillers; the interactions among the polymers, fillers, and penetrates; and the nature of penetrates, such as the gas molecular sizes. According to eqs. (2–4), the gas selectivities of the MMMs are not affected by the fillers and are the same as those of the pristine polymer membranes.

EXPERIMENTAL

Materials

Pebax MH 1657 [Pebax 1657, consisting of 60 wt % poly(ethylene oxide) and 40 wt % polyamide 6, density = 1.14 g/cm^3] was purchased from Arkema, Inc. GO (diameter = 1–5 μm, thickness = 0.8–1.2 nm) was purchased from Nanjing XFNANO Material Tech Co., Ltd. A mixture of ethanol and water (70/30 wt %) was used as a solvent for Pebax. Ethanol (analytical grade) was provided by Sinopharm Chemical Reagent Co., Ltd. Pure CO_2, CH_4, H_2, and N_2 were supplied by Dalian Gases Co. All of the materials were used as received.

Membrane Preparation

The membranes were prepared with a solution casting method. Pebax (1.8 g) was added to the ethanol/water mixture (40 mL) to prepare the Pebax solution at about 80°C under reflux and with vigorous stirring for 4 h. GO was dispersed in deionized water and then ultrasonicated for 6–18 h to form a suspension of GO, and the GO/H_2O concentration was 1–3.6 mg/mL. The mass ratios of GO to Pebax (Y) were 0 : 100–8 : 100, and the compositions of the Pebax/GO MMMs are denoted as P100G0–P100G8, accordingly. After the Pebax solution was cooled to ambient temperature, the Pebax solution and GO aqueous dispersion were mixed and stirred slowly for at least 5 h at ambient temperature. Then, the mixed solution was cast into a Teflon ring mold, and the solvent was evaporated at about 40°C. After the membranes were formed, they were dried in a vacuum oven at 50°C for at least 3 days to remove the residual solvent, and then, the dried membranes were held in a vacuum oven at ambient temperature. The membranes thicknesses were 65–85 μm. Here, the density of GO was assumed to be 2.28 g/cm^3,[17] so ϕ of GO could be calculated with eq. (5):

$$\phi = \frac{m_{GO}/\rho_f}{m_{GO}/\rho_f + m_{Pebax}/\rho_0} = \frac{Y/2.28}{Y/2.28 + 1/1.14} \quad (5)$$

where m_{GO} and m_{Pebax} are the masses of GO and Pebax, respectively, and ρ_f and ρ_0 are the densities of GO and Pebax, respectively.

Membrane Characterization

The crystalline properties of the Pebax/GO MMMs were measured with a wide-angle X-ray diffractometer (X'Pert Pro-1) with Cu Kα radiation ($\lambda = 1.5406$ Å).

The morphologies of the Pebax/GO MMMs were observed with a field emission scanning electron microscope (Quanta 200FEG). The samples were fractured in liquid nitrogen and then coated with gold by a sputtering method.

FTIR spectra of GO and Pebax/GO MMMs were obtained in attenuated total refection mode with an Equinox 55 FTIR spectrometer.

Stress–Strain Tests

Stress–strain measurements were conducted via a Reger universal material testing system at room temperature. Specimens with a gauge length of 20 mm and a width of 5 mm were used, and the thickness of the specimens was determined with a thickness tester. The test speed was 10 mm/min. The results are the average values of several measurements.

Gas-Permeation Measurements

The gas-permeation properties of the Pebax/GO MMMs were determined with a constant-volume/variable-pressure technique. The permeate side of the membrane was evacuated before each test. The permeation properties of the pure N_2, CH_4, H_2, and CO_2 were studied. The gas permeabilities and diffusion coefficients could be calculated with eqs. (6) and (7):

$$P = \frac{1}{76}\frac{273.15}{T}\frac{V}{A}\frac{l}{\Delta p}\frac{dp}{dt} \quad (6)$$

$$D = \frac{l^2}{6\theta} \quad (7)$$

where P is the gas permeability [Barrer; 1 Barrer = 10^{-10} cm^3(STP) cm (cm^2·s·cmHg)$^{-1}$], V is the downstream volume (cm^3), A is the area of the membrane (cm^2), T is the operating temperature (K), Δp is the transmembrane pressure difference (cmHg), l is the membrane thickness (cm), dp/dt is the rate of pressure increase measured by a pressure sensor in the downstream chamber (cmHg/s), D is diffusion coefficient (cm^2/s), and θ is the diffusion time lag (s). The relative standard deviation of gas permeabilities were calculated by the following equation, and the relative standard deviation of the gas permeabilities was within 10%:

$$\frac{\Delta P}{|P|} = \frac{|\Delta V|}{V} + \frac{|\Delta A|}{A} + \frac{|\Delta T|}{T} + \frac{|\Delta l|}{l} + \frac{|\Delta(\Delta p)|}{\Delta p} + \frac{|\Delta(dp/dt)|}{dp/dt} \quad (8)$$

The ideal selectivity (α) of one penetrant (subscript A) over another (subscript B) is given by eq. (9):

$$\alpha_{A/B} = \frac{P_A}{P_B} \quad (9)$$

where P_A and P_B are the permeability of penetrant A and penetrant B, respectively.

RESULTS AND DISCUSSION

Physical Properties of the Pebax/GO MMMs

XRD was used to determine the crystalline properties of the Pebax/GO MMMs, and the results are shown in Figure 3. The

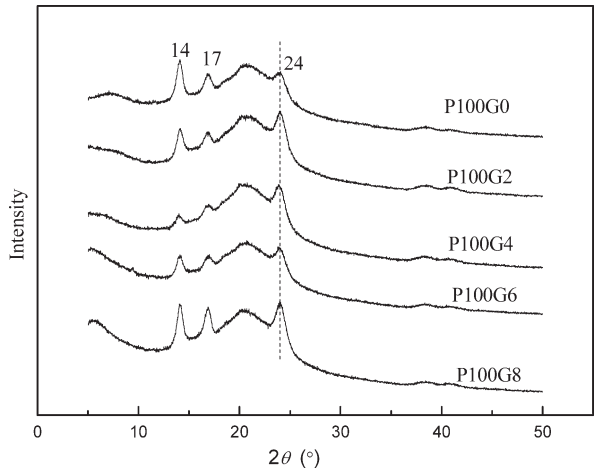

Figure 3. XRD patterns of Pebax/GO MMMs.

pristine Pebax membrane (P100G0) was a semicrystalline polymer with diffraction peaks at 14, 17, and 24° of 2θ, and the peak at 2θ = 24° resulted from the crystalline region of the PA segment by hydrogen bonding.[37] All of the Pebax/GO MMMs showed similar XRD patterns; this proved that GO did not destroy the semicrystalline structure of Pebax. It has been reported that the characteristic peak of GO was at a 2θ of 11°.[19,21] However, this was not observed in the Pebax/GO MMMs, which were similar to the poly(vinyl alcohol)/GO MMMs observed by Liang *et al.*[19] and Xu *et al.*[24] Exfoliated GO, in the monolayer form, showed no intensity characteristic peaks.[38] So, the results proved that GO was well exfoliated and uniformly dispersed in the polymer matrix.[19,24] The intensity of the diffraction peak at 2θ = 24° of the Pebax/GO MMMs was higher than that of the pristine Pebax membrane; this indicated that GO acted as a nucleating agent and induced the increase of crystallinity just like in multiwalled carbon nanotubes.[39]

The FTIR spectra of GO, P100G0, and P100G8 were detected and are shown in Figure 4. For GO, the characteristic peaks around 3265, 1730, 1556, and 1342 cm^{-1} were the stretching vibrations of O—H, C═O, and C═C and the bending vibrations of C—OH, respectively;[40,41] this suggested that there were at

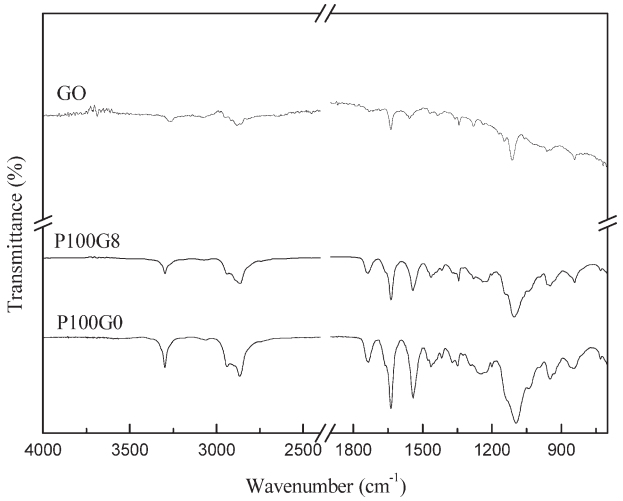

Figure 4. FTIR spectra of GO, P100G0 MMM, and P100G8 MMM.

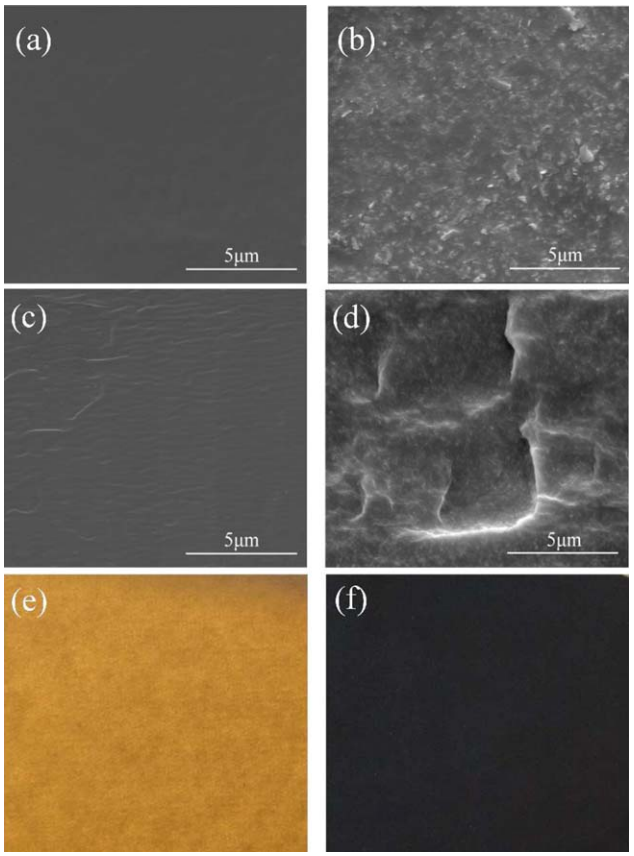

Figure 5. (a,b) Surface scanning electron microscopy images, (c,d) cross-sectional scanning electron microscopy images, and (e,f) digital pictures of Pebax/GO MMMs: (a) P100G0, (b) P100G3, (c) P100G0, (d) P100G3, (e) P100G3, and (f) P100G8. [Color figure can be viewed in the online issue, which is available at wileyonlinelibrary.com.]

least some hydroxyl and carboxyl groups in GO. The peak at 1111 cm^{-1} represented the stretching vibrations of C—O.[42] The stretching vibrations at 2872 cm^{-1} suggested the presence of aliphatic C—H groups, which was consistent with a nonaromatic carbon structure in GO.[41,42]

For the pristine Pebax, the peaks at 3296 and 1097 cm^{-1} represented the stretching vibrations of N—H and C—O, respectively.[37] The peak at 1740 cm^{-1} was assigned to the free C═O, and the peak at 1641 cm^{-1} indicated the presence of hydrogen-bonded C═O in H—N—C═O.[37,43]

The characteristic peaks of GO were not shown clearly in the spectrum of P100G8, which might have been because they were so weak that they were overlapped by those strong peaks of Pebax. On the other hand, because some of the Pebax matrix was present on the surface of GO, the spectrum of GO might not have been detected, and only that of Pebax was shown.

The morphologies of the Pebax/GO MMMs are shown in Figure 5. Compared with that of P100G3 [Figure 5(b)], the surface of P100G0 [Figure 5(a)] was much smoother. As shown in Figure 5(b,d), GO was in the form of flakes, and it seemed that GO was well dispersed in the Pebax matrix. This was consistent with the XRD analysis. This suggested that the agglomeration of GO was inhibited with the aids of functionalization and

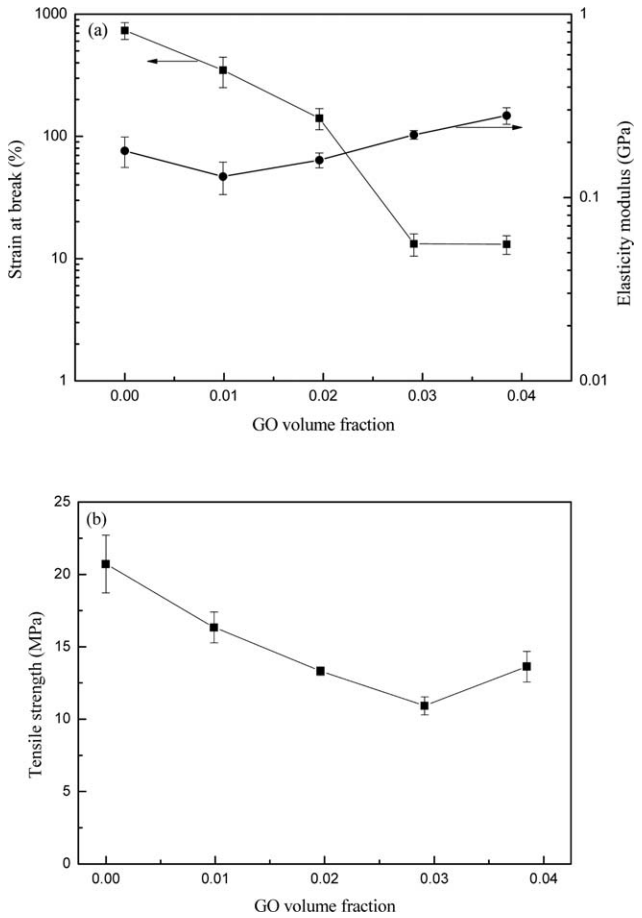

Figure 6. Influence of the GO content on the mechanical properties of the Pebax/GO MMMs.

ultrasonic treatment. The color of the Pebax/GO MMMs with less GO was golden, such as that of P100G3 shown in Figure 5(e). With increasing GO, the Pebax/GO MMMs became darker in color; for example, P100G8, shown in Figure 5(f), was dark brown.

Mechanical Properties of the Pebax/GO MMMs

The mechanical properties of the Pebax/GO MMMs were evaluated by stress–stain tests, which are shown in Figure 6. As shown in Figure 6(a), with increasing GO content, the stain at break decreased, whereas the elasticity modulus increased. For the Pebax/GO MMMs with 3.85 vol % GO (P100G8), the strain at break decreased by 98%, and the elasticity modulus increased by 56%. This suggested that the Pebax/GO MMMs were more brittle and rigid than the pristine Pebax membrane.[44] Because the elasticity modulus was used to characterize the resistance to elastic deformation, the higher elasticity modulus of the Pebax/GO MMMs indicated that the incorporation of GO was beneficial for the improvement of the antideformation capacity of the Pebax/GO MMMs. The tensile strength decreased by 34% at a 3.85 vol % GO loading [Figure 6(b)]; this suggested that the incorporation of GO inhibited the molecular rearrangement and orientation during deformation[45] and that the interaction between GO and Pebax was not strong enough to enhance the tensile strength.[19]

Gas-Permeation Properties of the Pebax/GO MMMs

Figure 7 shows the influence of the pressure on the gas permeabilities of the P100G4 MMMs. It was clear that the relationship between the gas permeability and pressure could be expressed with the following linear equation:[46]

$$P = P_{\Delta p=0}(1 + n\Delta p) \quad (10)$$

where $P_{\Delta p=0}$ is the gas permeability when Δp is 0 (i.e., infinite dilution permeability) and n is an adjustable constant that characterizes the effect of pressure on gas permeability.

Just as that shown in Figure 7, the CO_2 permeability increased with pressure, so the n value was positive for CO_2; this was induced by plasticization. For H_2, CH_4, and N_2, the permeabilities were influenced little by the pressure, and the n values were a little negative because of the hydrostatic compression effect.[47] The n values of the Pebax/GO MMMs for CO_2, N_2, H_2, and CH_4 are listed in Table I. Compared with the pristine Pebax membrane, the n values for CO_2 became larger, and the absolute values of n for H_2, CH_4, and N_2 became smaller with increasing GO content. This suggested that the plasticization of CO_2 increased, whereas the hydrostatic compressive effect of H_2, CH_4, and N_2 decreased. In fact, the increased crystallinity and more rigid nature of the Pebax/GO MMMs contributed to the changes in the n values. The increased crystallinity and the more rigid nature of the MMMs made the fractional free volume decrease and resulted in a smaller hydrostatic compressive effect and subsequently made the absolute values of n for H_2, CH_4, and N_2 become smaller. For CO_2, n was determined by the plasticization and hydrostatic pressure; a lower hydrostatic compressive effect made the increase of CO_2 with pressure more obvious. Namely, the plasticization effect became more obvious.

The influence of the temperature on the gas permeability is shown in Figure 8. The gas permeabilities increased with temperature. For CO_2, its solubility in the rubbery polymer decreased with increasing temperature; however, for H_2 and N_2, the solubility increased with increasing temperature.[48] Therefore, in particular for CO_2, the diffusivity made a great

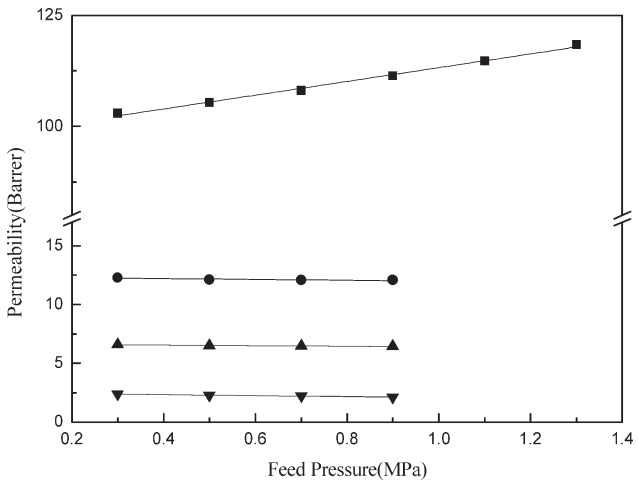

Figure 7. Influence of the pressure on the permeabilities of (■) CO_2, (●) H_2, (▲) CH_4, and (▼) N_2 for P100G2 MMM at 35°C.

Table I. *n* Values of the Pebax/GO MMMs for CO_2, N_2, H_2, and CH_4 at 35°C

	P100G0 (0 vol % GO)	P100G2 (0.99 vol % GO)	P100G4 (1.96 vol % GO)	P100G6 (2.91 vol % GO)	P100G8 (3.85 vol % GO)
CO_2	0.16	0.16	0.17	0.18	0.18
N_2	−0.15	−0.17	−0.11	−0.093	−0.12
H_2	−0.052	−0.029	−0.035	−0.025	−0.027
CH_4	−0.058	−0.035	−0.047	−0.022	−0.037

The relative standard deviation of *n* was within 10%.

contribution to the increase in the gas permeability with temperature. There was a linear relationship between the logarithm of the gas permeability and the reciprocal of the temperature; this could be expressed by the Arrhenius equation:

$$P = P_o \exp\left[\frac{-E_p}{RT}\right] \quad (11)$$

where P_0 is the pre-exponential factor, E_p is the apparent activation energy for permeation (kJ/mol), R is the gas constant (8.314 $J \cdot K^{-1} \cdot mol^{-1}$), and T is the absolute temperature (K).

Table II lists the E_p values of the Pebax/GO MMMs for CO_2, N_2, H_2, and CH_4. The E_p of CO_2 was the smallest; this was contributed by its interaction with the poly(ethylene oxide) segment and its high condensability, which was characterized by the critical temperature (the critical temperatures of CO_2, N_2, H_2, and CH_4 were 304.2, 126.2, 33.2, and 190.6 K, respectively). Compared with that of the pristine Pebax membrane, the E_p values of the Pebax/GO MMMs for CO_2, N_2, H_2, and CH_4 increased with the addition of GO. This might have been because the polymer chains were more difficult to rotate when GO was incorporated, and this resulted in a higher activation energy for diffusion.[37]

Figure 9 shows the influence of the GO content on the permeabilities of CO_2, H_2, CH_4, and N_2. With increasing GO content, the permeabilities of CO_2, H_2, CH_4, and N_2 all gradually decreased. For the Pebax/GO MMMs with 3.85 vol % GO (P100G8), the permeabilities of CH_4, CO_2, and N_2 decreased by 74, 70, and 69%, respectively, compared to that of the pristine Pebax membrane. So, the selectivities of CO_2/N_2 and CO_2/CH_4 did not change much (shown in Figure 10); this was consistent with the model prediction from eq. (4). The structural changes in the membranes, such as the chain flexibility, had a minor effect on H_2 compared to their effects other gases because of hydrogen's small size,[31] as shown later in Table IV, so the H_2 permeability only decreased by about 59% at 3.85 vol % GO loading. As a result, the CO_2/H_2 selectivity decreased by 27%, and the H_2/CH_4 selectivity increased by 56%. The remarkable decrease in the gas permeabilities for the Pebax/GO MMMs illustrated that GO inhibited gas diffusion and formed a diffusion barrier in the polymer matrix.[17] First, the addition of impermeable GO decreased the available diffusion area because of the replacement of permeable Pebax by impermeable GO.[36] Second, the diffusion tortuosity became greater, and the gas diffusion channel was restricted after GO was incorporated.[37] The diffusivities of larger gases decreased to a greater extent than those of smaller gases,[13] and this also illustrated the changes in the gas selectivities, shown in Figure 10. Meanwhile, the increase in the crystallinity caused by the incorporation of GO, shown in Figure 3, also contributed to the decrease in the gas permeabilities. The θ of CH_4 for the Pebax/GO MMMs are shown in Figure 11; they clearly explain the gas-diffusion properties of the Pebax/GO MMMs with different GO contents. As shown in Figure 11, with increasing GO content, θ/l^2 l was the membrane thickness for CH_4 increased. According to eq. (7), the gas diffusivity is inversely proportional to θ/l^2, so the CH_4 diffusivity decreased with increasing GO content. At present, the representative gas membrane materials mainly include PDMS, cellulose acetate, polyimide, and so on, and their permeation properties are listed in Table III for a comparison with the Pebax/GO MMMs. The Pebax/GO MMMs had high CO_2/N_2 and CO_2/H_2 selectivities.

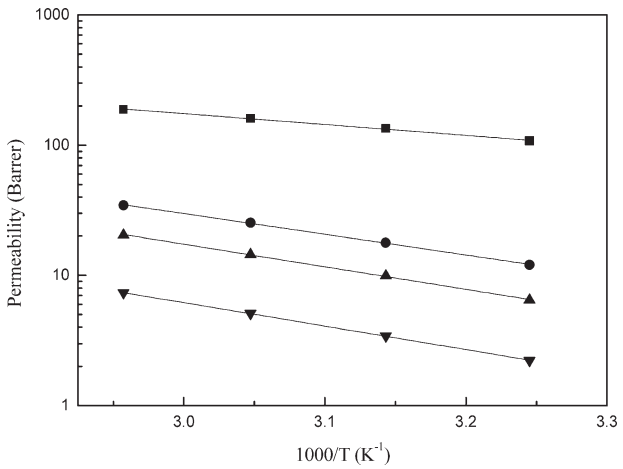

Figure 8. Influence of the temperature on the permeabilities of (■) CO_2, (●) H_2, (▲) CH_4, and (▼) N_2 for P100G2 MMM at 0.7 MPa.

Table II. E_p Values of the Pebax/GO MMMs for CO_2, N_2, H_2, and CH_4 at 0.7 MPa

	P100G0	P100G2	P100G4	P100G5	P100G8
CO_2	16.5	16.0	19.8	22.7	23.7
N_2	35.6	34.5	42.1	43.3	44.8
H_2	30.8	30.4	35.5	36.3	36.7
CH_4	34.1	33.2	40.3	42.3	43.0

The relative standard deviation of E_p was within 5%.

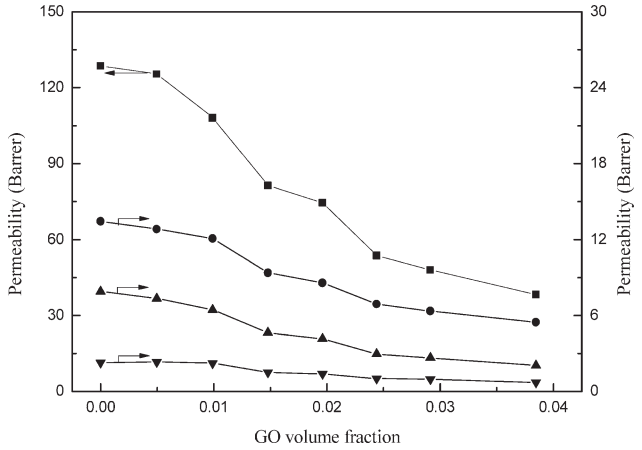

Figure 9. Influence of the GO content on the permeabilities of (■) CO_2, (●) H_2, (▲) CH_4, and (▼) N_2 for Pebax/GO MMMs at 35°C and 0.7 MPa.

Prediction of the Gas-Permeation Properties for the Pebax/GO MMMs

Figure 12 shows the experimental and model predicted normalized permeabilities for the Pebax/GO MMMs. GO was impermeable to all gases, so the permeation properties of the Pebax/GO MMMs could be described with eq. (2) or (4). For the Maxwell model described in eq. (2), the predicted normalized permeabilities almost did not change with increasing GO content from 0 to 4 vol %, and there was a big deviation between the experimental and predicted values. That is to say, the Maxwell model could not predict the transport properties of CO_2, N_2, H_2, and CH_4 for the Pebax/GO MMMs. Unlike in the Maxwell model, the geometrical shape of the fillers was considered in the Lape model with the A_f parameter. The experimental values of CO_2, N_2, H_2, and CH_4 were well fitted with the Lape model; this suggested that the geometrical shape of the filler played an important role in the transport process of the gases. For the Pebax/GO MMMs, the values of P_{MMMs}/P_0 for different gases and ϕ of GO could be calculated, so the A_f values of CO_2, N_2, H_2, and CH_4 could be regressed with Origin software according to the Lape model. The

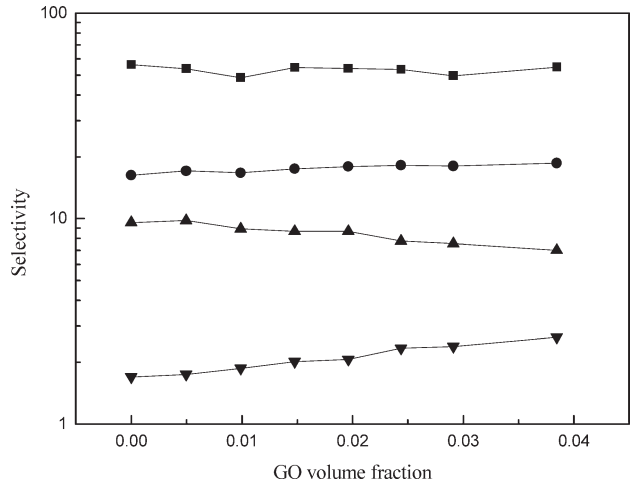

Figure 10. Influence of the GO content on the selectivities of (■) CO_2/N_2, (●) CO_2/CH_4, (▼) H_2/CH_4, and (▲) CO_2/H_2 for the Pebax/GO MMMs at 35°C and 0.7 MPa.

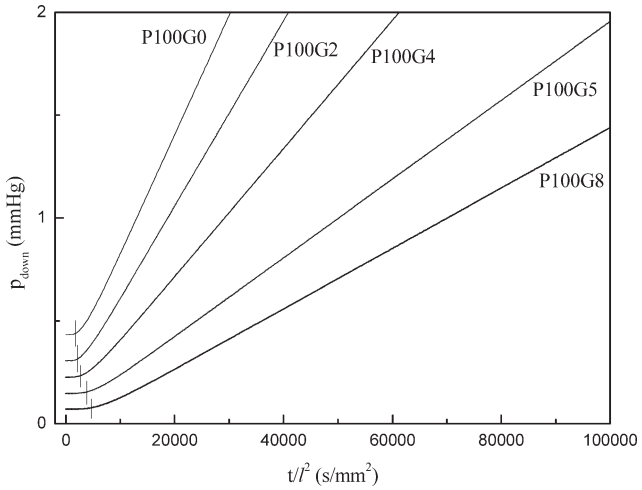

Figure 11. Gas-permeation curves of the Pebax/GO MMMs for CH_4 at 35°C and 0.7 MPa: p_{down} was the pressure of downstream chamber, t was the permeation time.

values of A_f are shown in Table IV, and small deviations for CO_2, N_2, H_2, and CH_4 was observed. Theoretically, A_f should have been a constant value for the Pebax/GO MMMs; this was not relevant to penetrates. However, on the basis of the assumption of a parallel regular array of the fillers, the Lape model does not consider the size distribution and random orientation of fillers, the physical properties of the penetrates (e.g., molecular size), and the interaction among polymers, fillers, and penetrates; these might have caused some deviation of the A_f values for CO_2, N_2, H_2, and CH_4. As shown in Table IV, A_f increased with increasing gas critical volume. Thus, the impermeable GO had a larger inhibition on the transport of larger gases. An average A_f of 86 for CO_2, N_2, H_2, and CH_4 was calculated by the regression of the normalized permeabilities of different gases with the Lape model. It seemed that the transport properties of the Pebax/GO MMMs could be described successfully by this model. Obviously, the A_f value from the Lape model (86) was much lower than its theoretical value. The ultrasound destruction, layer misalignment, stacking of the flakes, and random orientation of the flakes might have led to a lower effective A_f.[17,50]

To observe the influence of the geometrical shape of the fillers on the permeation properties of different MMMs, the CO_2 normalized permeabilities of the Pebax membranes with different fillers, such as SAPO-34,[51] amino-modified multiwalled carbon nanotubes (MWNTs-NH_2),[52] and GO, are shown in Figure 13. MWNTs-NH_2 was highly permeable to gases; thus, $P_f = \infty$ could be assumed, and the permeation properties of the Pebax/MWNTs-NH_2 MMMs could be described with eq. (3). As shown in Figures 12(a) and 13(a1), the experimental P_{MMMs}/P_0 values were a little higher than those predicted with eq. (3). The difference might have been due to the voids between the tangled MWNTs-NH_2s.[52] For SAPO-34, its CO_2 permeability was assumed to be 600 Barrer,[53] and the permeation properties of the Pebax/SAPO-34 MMMs could be described with eq. (1). As shown in Figure 13(b,b1), the experimental P_{MMMs}/P_0 values were lower than the predicted values at low SAPO-34 contents, and they were higher than the predicted values when the

Table III. Permeation Properties of the Pebax/GO MMMs and Representative Membrane Materials

Polymer	Temperature (°C)	Pressure (MPa)	P_{CO2} (Barrer)	P_{CO2}/P_{N2}	P_{CO2}/P_{CH4}	P_{CO2}/P_{H2}	Reference
PDMS	35	0	3800	9.5	3.2	4.3	47
Cellulose acetate	35	0.03	6.0	25.8	29.2	0.4	49
Matrimid	35	1	4.5	—	34.0	—	1
P100G0	35	0.7	128.6	56.2	16.3	9.6	This study
P100G2	35	0.7	108.0	48.5	16.7	8.9	This study
P100G5	35	0.7	53.7	53.2	18.2	7.8	This study
P100G8	35	0.7	38.3	54.8	18.6	7.0	This study

SAPO-34 content increased. The difference might have resulted from the increase in the tortuosity for diffusion at low SAPO-34 contents, whereas for high SAPO-34 contents, defects occurring in the membranes, such as phase separation, might have accounted for the difference.[51] For GO, unlike MWNTs-NH_2 and SAPO-34, the experimental P_{MMMs}/P_0 values of the Pebax/GO MMMs dramatically decreased with increasing GO content. When Figures 13(c), 13(c1), and 13(c2) are compared, as mentioned in Figure 12, the experimental P_{MMMs}/P_0 values of the Pebax/GO MMMs were in good agreement with the Lape model predictions with $A_f = 86$ compared to those of the Maxwell model. With the Maxwell model, the derivation between the experimental and predicted values of the Pebax/GO MMMs were much larger than those of the Pebax/MWNTs-NH_2 MMMs and Pebax/SAPO-34 MMMs. The big derivation of the Pebax/GO MMMs could not be explained only by the changes in the membrane structure, and the geometrical shape of GO had to be considered. Therefore, the geometrical shape of the fillers played an important role in their permeation properties.

Table IV. Apparent A_f Values Determined from the Fit of the Experimental Normalized Permeability Curves by the Lape Model

	H_2	N_2	CO_2	CH_4
V_c (cm^3/mol)[a]	65.1	89.8	93.9	99.2
A_f[b]	74 (±3)	82 (±5)	90 (±3)	100 (±3)
$\bar{A}_f$[b]	86 (±3)			

[a] V_c, critical volume from ref. 47.
[b] Values in parentheses are standard errors.

CONCLUSIONS

Pebax/GO MMMs were prepared with the solution casting method, and their gas-separation performance and mechanical properties were investigated. With ultrasonic treatment, GO was well dispersed in the Pebax matrix, and its incorporation induced increases in the crystallinity and elasticity modulus for the Pebax/GO MMMs, whereas the strain at break and tensile strength decreased. Compared with that in the pristine Pebax membrane, the plasticization of CO_2 in the Pebax/GO MMMs increased, whereas the hydrostatic compressive effect of H_2, CH_4, and N_2 decreased. The E_p values of CO_2, N_2, H_2, and CH_4 all increased for the Pebax/GO MMMs. Because of the

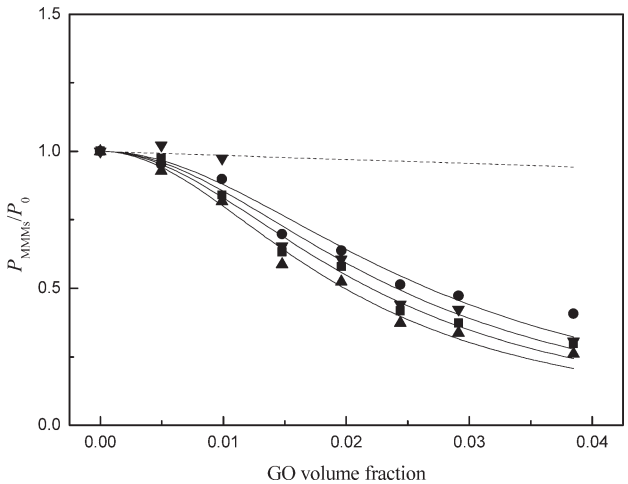

Figure 12. Comparison of the experimental values and model predictions of the normalized permeabilities of (•) H_2, (▼) N_2, (■) CO_2, and (▲) CH_4 for the Pebax/GO MMMs. The solid curves are regression lines based on the Lape model [eq. (4)]; the dashed line is a prediction line based on the Maxwell model [eq. (2)].

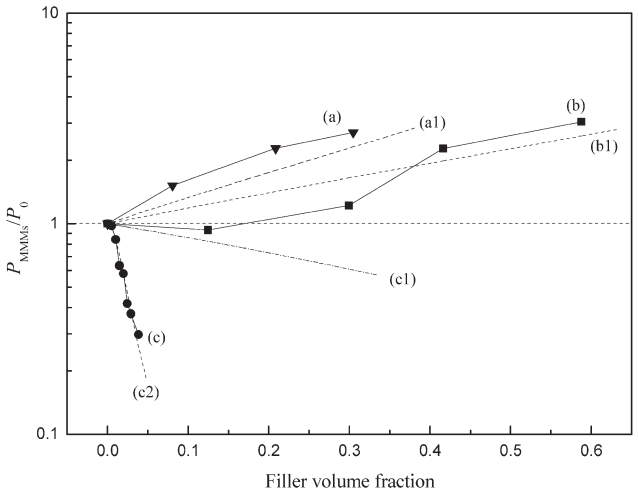

Figure 13. Influence of the geometrical shape of the fillers on the CO_2-normalized permeability at 35°C and 0.7 MPa (the solid curves were obtained from experimental values from the laboratory): (a) MWNTs-NH_2 as the filler, (b) SAPO-34 as the filler, and (c) GO as the filler. The dashed curves were predicted according to models: (a1) predicted by eq. (3), (b1) predicted by eq. (1) with $P_f = 600$ Barrer, (c1) predicted by eq. (2), and (c2) predicted by eq. (4) with $A_f = 86$.

impermeable nature of GO, the gas permeabilities of the Pebax/GO MMMs remarkably decreased with increasing GO content. Compared with the pristine Pebax membrane, the CO_2 permeability of the Pebax/GO MMMs with 3.85 vol % GO decreased by about 70%. For the Pebax/GO MMMs, the Maxwell model could not predict the gas-transport properties because the geometrical shape of GO played an important role in the permeation process. With the introduction of A_f, the gas permeabilities of the Pebax/GO MMMs could be described successfully by the Lape model with an average A_f of 86.

ACKNOWLEDGMENTS

Financial support from the National Science and Technology Planning Project (contract grant number 2011BAC08B00) and the National High Technology Research and Development Program of China (863 Program; contract grant number 2012AA03A611) is gratefully acknowledged.

REFERENCES

1. Peydayesh, M.; Asarehpour, S.; Mohammadi, T.; Bakhtiari, O. *Chem. Eng. Res. Des.* **2013**, *91*, 1335.
2. Jia, M.-D.; Pleinemann, K.-V.; Behling, R.-D. *J. Membr. Sci.* **1992**, *73*, 119.
3. Savoji, H.; Rana, D.; Matsuura, T.; Soltanieh, M.; Tabe, S. *J. Appl. Polym. Sci.* **2012**, *124*, 2300.
4. Savoji, H.; Rana, D.; Matsuura, T.; Soltanieh, M.; Tabe, S. *J. Appl. Polym. Sci.* **2012**, *124*, 2287.
5. Chung, T. S.; Jiang, L. Y.; Li, Y.; Kulprathipanja, S. *Prog. Polym. Sci.* **2007**, *32*, 483.
6. Rana, D.; Matsuura, T. In Encyclopedia of Membrane Science and Technology; Hoek, E. M. V., Tarabara; V. V., Eds.; Wiley: Hoboken, NJ, **2013**; Vol. *3*, p 1668.
7. Qiao, X. Y.; Chung, T. S.; Rajagopalan, R. *Chem. Eng. Sci.* **2006**, *61*, 6816.
8. Basu, S.; Cano-Odena, A.; Vankelecom, I. F. *J. Sep. Purif. Technol.* **2011**, *81*, 31.
9. Vu, D. Q.; Koros, W. J.; Miller, S. J. *J. Membr. Sci.* **2003**, *211*, 311.
10. Ahmad, A. L.; Jawad, Z. A.; Low, S. C.; Zein, S. H. S. *J. Membr. Sci.* **2014**, *451*, 55.
11. He, Z. J.; Pinnau, I.; Morisato, A. *Desalination* **2002**, *146*, 11.
12. Sun, H.; Ma, C.; Yuan, B.; Wang, T.; Xu, Y.; Xue, Q.; Li, P.; Kong, Y. *Sep. Purif. Technol.* **2014**, *122*, 367.
13. Chung, T.-S.; Chan, S. S.; Wang, R.; Lu, Z.; He, C. *J. Membr. Sci.* **2003**, *211*, 91.
14. Geim, A. K.; Novoselov, K. S. *Nat. Mater.* **2007**, *6*, 183.
15. Lee, C.; Wei, X.; Kysar, J. W.; Hone, J. *Science* **2008**, *321*, 385.
16. Bunch, J. S.; Verbridge, S. S.; Alden, J. S.; van der Zande, A. M.; Parpia, J. M.; Craighead, H. G.; McEuen, P. L. *Nano Lett.* **2008**, *8*, 2458.
17. Kim, H.; Miura, Y.; Macosko, C. W. *Chem. Mater.* **2010**, *22*, 3441.
18. Roy, I.; Rana, D.; Sarkar, G.; Bhattacharyya, A.; Saha, N. R.; Mondal, S.; Pattanayak, S.; Chattopadhyay, S.; Chattopadhyay, D. *RSC Adv.* **2015**, *5*, 25357.
19. Liang, J.; Huang, Y.; Zhang, L.; Wang, Y.; Ma, Y.; Guo, T.; Chen, Y. *Adv. Funct. Mater.* **2009**, *19*, 2297.
20. Zinadini, S.; Zinatizadeh, A. A.; Rahimi, M.; Vatanpour, V.; Zangeneh, H. *J. Membr. Sci.* **2014**, *453*, 292.
21. Roy, I.; Bhattacharyya, A.; Sarkar, G.; Saha, N. R.; Rana, D.; Ghosh, P. P.; Palit, M.; Das, A. R.; Chattopadhyay, D. *RSC Adv.* **2014**, *4*, 52044.
22. Stankovich, S.; Dikin, D. A.; Dommett, G. H.; Kohlhaas, K. M.; Zimney, E. J.; Stach, E. A.; Piner, R. D.; Nguyen, S. T.; Ruoff, R. S. *Nature* **2006**, *442*, 282.
23. Liu, L. Q.; Barber, A. H.; Nuriel, S.; Wagner, H. D. *Adv. Funct. Mater.* **2005**, *15*, 975.
24. Xu, Y.; Hong, W.; Bai, H.; Li, C.; Shi, G. *Carbon* **2009**, *47*, 3538.
25. Steurer, P.; Wissert, R.; Thomann, R.; Muelhaupt, R. *Macromol. Rapid Commun.* **2009**, *30*, 316.
26. Kim, H.; Macosko, C. W. *Polymer* **2009**, *50*, 3797.
27. Kim, H.; Macosko, C. W. *Macromolecules* **2008**, *41*, 3317.
28. Kim, J. H.; Ha, S. Y.; Lee, Y. M. *J. Membr. Sci.* **2001**, *190*, 179.
29. Bondar, V. I.; Freeman, B. D.; Pinnau, I. *J. Polym. Sci. Part B: Polym. Phys.* **2000**, *38*, 2051.
30. Reijerkerk, S. R.; Knoef, M. H.; Nijmeijer, K.; Wessling, M. *J. Membr. Sci.* **2010**, *352*, 126.
31. Car, A.; Stropnik, C.; Yave, W.; Peinemann, K.-V. *J. Membr. Sci.* **2008**, *307*, 88.
32. Car, A.; Stropnik, C.; Yave, W.; Peinemann, K.-V. *Sep. Purif. Technol.* **2008**, *62*, 110.
33. Feng, S. C.; Ren, J. Z.; Li, H.; Hua, K. S.; Li, X. X.; Deng, M. C. *J. Energy Chem.* **2013**, *22*, 837.
34. Wijmans, J. G.; Baker, R. W. *J. Membr. Sci.* **1995**, *107*, 1.
35. Bouma, R. H. B.; Checchetti, A.; Chidichimo, G.; Drioli, E. *J. Membr. Sci.* **1997**, *128*, 141.
36. Lape, N. K.; Nuxoll, E. E.; Cussler, E. L. *J. Membr. Sci.* **2004**, *236*, 29.
37. Kim, J. H.; Lee, Y. M. *J. Membr. Sci.* **2001**, *193*, 209.
38. Tang, H.; Ehlert, G. J.; Lin, Y.; Sodano, H. A. *Nano Lett.* **2012**, *12*, 84.
39. Choi, J. H.; Jegal, J.; Kim, W. N. *Macromol. Symp.* **2007**, *249*, 610.
40. Ganesh, B. M.; Isloor, A. M.; Ismail, A. F. *Desalination* **2013**, *313*, 199.
41. Hontoria-Lucas, C.; López-Peinado, A. J.; López-González, J. D. D.; Rojas-Cervantes, M. L.; Martín-Aranda, R. M. *Carbon* **1995**, *33*, 1585.
42. Murali, R. S.; Sridhar, S.; Sankarshana, T.; Ravikumar, Y. V. L. *Ind. Eng. Chem. Res.* **2010**, *49*, 6530.

43. Semsarzadeh, M. A.; Sadeghi, M.; Barikani, M. *Iran. Polym. J.* **2008**, *17*, 431.

44. Zoppi, R. A.; das Neves, S.; Nunes, S. P. *Polymer* **2000**, *41*, 5461.

45. Nguyen, D. A.; Lee, Y. R.; Raghu, A. V.; Jeong, H. M.; Shin, C. M.; Kim, B. K. *Polym. Int.* **2009**, *58*, 412.

46. Lin, H.; Freeman, B. D. *J. Membr. Sci.* **2004**, *239*, 105.

47. Merkel, T. C.; Bondar, V. I.; Nagai, K.; Freeman, B. D.; Pinnau, I. *J. Polym. Sci. Part B: Polym. Phys.* **2000**, *38*, 415.

48. Van Amerongen, G. J. *J. Appl. Phys.* **1946**, *17*, 972.

49. Li, J. T.; Wang, S. C.; Nagai, K.; Nakagawa, T.; Mau, A. W. H. *J. Membr. Sci.* **1998**, *138*, 143.

50. Bharadwaj, R. K. *Macromolecules* **2001**, *34*, 9189.

51. Zhao, D.; Ren, J. Z.; Li, H.; Hua, K. S.; Deng, M. C. *J. Energy Chem.* **2014**, *23*, 227.

52. Zhao, D.; Ren, J. Z.; Li, H.; Li, X. X.; Deng, M. C. *J. Membr. Sci.* **2014**, *467*, 41.

53. Hong, M.; Li, S. G.; Falconer, J. L.; Noble, R. D. *J. Membr. Sci.* **2008**, *307*, 277.